EUROFUSION WPMST1-CP(16) 15174

F Reimold et al.

Analysis of the impact of nitrogen- & neon-seeding on ASDEX-Upgrade H-Modes with SOLPS simulations

Preprint of Paper to be submitted for publication in
Proceedings of 26th IAEA Fusion Energy Conference

This work has been carried out within the framework of the EUROfusion Consortium and has received funding from the Euratom research and training programme 2014-2018 under grant agreement No 633053. The views and opinions expressed herein do not necessarily reflect those of the European Commission.

Analysis of the impact of nitrogen- & neon-seeding on ASDEX Upgrade H-Modes with SOLPS simulations

F. Reimold[1], M.Wischmeier[2], A.S. Kukushkin[3,4], D.Reiter[1], M.Bernert[2], the ASDEX Upgrade Team* and the EUROfusion MST1 Team†

[1]Forschungszentrum Jülich GmbH, Trilateral Euregio Cluster, 52425 Jülich, Germany
[2]Max-Planck Institut for Plasma Physics, 85748 Garching, Germany
[3]NRC Kurchatov institut, Kurchatov sq. 1, 123182 Moscow, Russia
[4]NRNU MEPhI, Kashirskoje sh. 31, 115409 Moscow, Russia

Corresponding Author: f.reimold@fz-juelich.de

Abstract:
Future fusion devices like ITER and DEMO will have to be operated with a detached divertor to meet material limits. Stable H-mode operation at high heating power $P_{Heat}/R = 5 - 15$ MWm^{-1} with both targets completely detached has been demonstrated with nitrogen seeding in the all-tungsten ASDEX Upgrade tokamak. However, nitrogen is chemically active and significant amounts of ammonia are present in the pumped residual gas of nitrogen-seeded ASDEX Upgrade discharges. Gas handling in the ITER tritium plant would be simpler and hence cheaper if ammonia could be avoided in the residual gas and neon is discussed as a replacement seeding gas for nitrogen. Unfortunately, to date it has not been possible to establish a stable H-mode scenario with strong divertor cooling using neon seeding in ASDEX Upgrade. In this contribution, SOLPS modeling is used in order to evaluate the possibilities of neon seeding for power exhaust in ASDEX Upgrade. Simulations with nitrogen and neon as seeding species and otherwise identical input parameters are used to compare the effect of the different impurities as seeding species. The results indicate that for neon seeding a lower divertor enrichment of neon, longer mean free paths for neon neutrals and the radiation potential that is shifted to higher temperatures for neon lead to a higher fraction of the radiation coming from the main chamber. Similar divertor parameters can be achieved with both impurities, but at a higher degradation of the upstream separatrix pressure for neon.

*See author list of Ref. [1]
†See appendix of H. Meyer et.al. (OV/P-12) Proc. 26th IAEA Fusion Energy Conf. 2016, Kyoto, Japan

1 Introduction

Future fusion devices like ITER and DEMO will have to be operated with a detached divertor to meet material limits. Stable H-mode operation at high heating power $P_{Heat}/R = 5 - 15$ MW/m with both targets completely detached, confinement of $H_{98} = 0.8 - 1.05$ and Greenwald fraction of $f_{GW} = 0.7 - 0.9$ has been demonstrated with nitrogen seeding in the all-tungsten ASDEX Upgrade tokamak [2, 3, 4]. However, nitrogen is chemically active and significant amounts of ammonia are present in the pumped residual gas of nitrogen-seeded ASDEX Upgrade and JET-ILW discharges [5, 6, 7]. The issue of tritium retention in ammonia surface films in remote areas of the reactor and gas handling in the ITER tritium plant [**?**] would be simplified if large amounts of ammonia could be avoided in the residual gas. To this end neon is discussed as a replacement seeding gas for nitrogen in power exhaust applications [8, 9].In attempts to study neon seeding for power exhaust in ASDEX Upgrade experiments it has so far not been possible to establish a stable H-mode scenario with strong divertor cooling or detached targets. In these experiments a radiative collapse of the plasma occurs when neon starts to cool the divertor and the discharges finally disrupt. Initial analysis suggests that impurity accumulation from tungsten and neon is responsible for the radiative collapse [4]. This operational challenge for a neon-seeded scenario impeded a detailed experimental analysis of the power exhaust properties of neon in the specific conditions at ASDEX Upgrade. A direct comparison of experimental data with nitrogen- and neon-seeding is not (yet) possible. Instead, SOLPS modeling without a direct experimental reference is used in this contribution to compare neon and nitrogen as radiative species for power exhaust in H-mode simulations. These simulations have been derived from a validated simulation of a nitrogen-seeded H-mode discharge [3]. A set of cases with increasing nitrogen or neon seeding rates - leading from high-recycling to detached outer divertor targets - have been modeled and will be analyzed in this work. The modeling setup is presented in Section 2, the modeling results are presented in Section 3 and the paper closes with a discussion and a summary in Section 4.

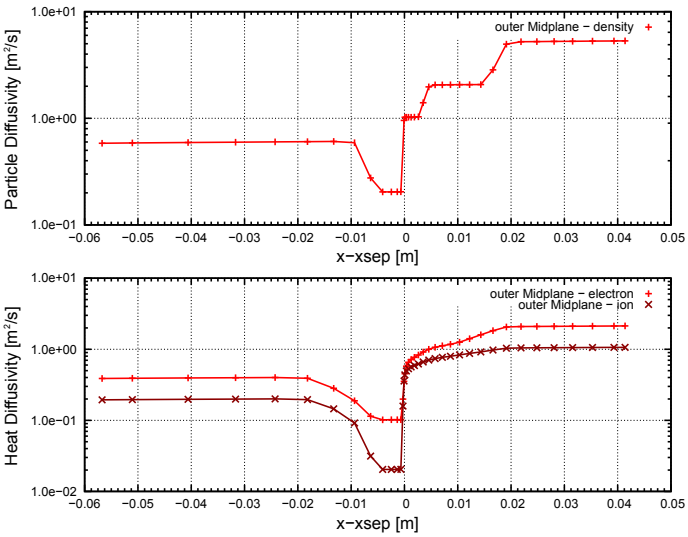

FIG. 1 – Perpendicular profiles of the transport coefficients $\chi_{e,i}$ and D.

2 Modeling Setup & Relation to Experiments

The presented simulations are derived from validated SOLPS modeling of a nitrogen seeded, medium heating power ($P_{Heat}/R = 5$ MWm^{-1}) discharge [10, 2, 3]. In this

study we limit ourselves to divertor states that have not yet developed the characteristic radiation at the X-point in the completely detached X-point radiation regime [2]. The code SOLPS5.0[1] is used for the modeling. The perpendicular transport coefficient profile at the outer midplane is given in Fig. 1. To account for the ballooning nature of transport the transport coefficients are rescaled in the poloidal plane by $B_{t,ref}^2/B_t^2$, where $B_{t,ref}$ is the average toroidal magnetic field in the simulations domain and the B_t is the local toroidal magnetic field. In the common flux region below the X-point the transport coefficients are increased by a factor of three to avoid numerical issues with the drift terms in this study. In the private flux region the transport coefficients are taken to be constant with $D = \chi_e = \chi_i = 3$ m^2/s.

Fall-off lengths for the electron and ion temperature $\lambda_T = 1.0$ cm and the density $\lambda_n = 0.75$ cm and a zero perpendicular shear condition for the Mach number were used as boundary conditions at the main chamber grid boundary. At the private-flux grid boundary $\lambda_T = 0.5$ cm, $\lambda_n = 0.25$ cm and a zero perpendicular shear condition for the Mach number were set. At the targets standard sheath boundary conditions with $\gamma_e = 3.0$ and $\gamma_i = 5.0$ for the heat flux, $v_\parallel \geq c_s$ for the parallel velocity and a zero parallel gradient for the density were employed. At the core grid boundary the heat flux into electrons and ions was specified to be equal with $P_{Heat,e/i} = 2.6$ MW. The particle flux across the core boundary was chosen to be zero for all species except for deuterium, which accounts for the net influx of 8.5×10^{21} s^{-1} due to NBI heating. A zero perpendicular gradient of the parallel velocity $v_\parallel$ was specified. The neutral atomic data model employed is very similar to Ref. [11]. The neutral domain model is calibrated to mimic the neutral conductances of the subdivertor structure [12, 13, 10] and a pumping speed of $S_{pump} = 114$ m^3/s of the ASDEX Upgrade pumps [**?**]. The recycling coefficient for all ions (D+N or D+Ne) is taken to be 1.0 (fully recycling) at all surfaces except for the pump surfaces,

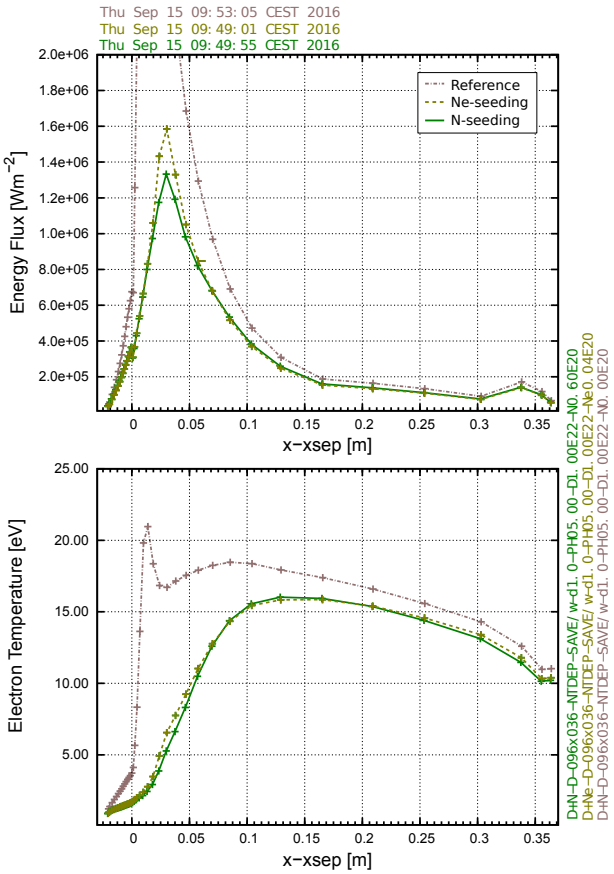

FIG. 2 – Similar outer target power flux and temperature profiles can be achieved with seeding nitrogen and neon. Power flux (top) and electron temperature (bottom) profiles are shown for a pure-D reference case (red dashed-dotted), a case with a Ne-seeding rate of 4×10^{18} s^{-1} *(yellow dashed) and a case with a N-seeding rate of* 6×10^{19} s^{-1} *(green solid).*

[1]Modified SVN Revision 4636 at `http://solps-mdsplus.aug.ipp.mpg.de/repos/SOLPS/trunk/solps5.0/`

where all particles are pumped with the same efficiency. At the cryopump surface the albedo is 0.81 and at the entrance surface to the pumping duct towards the turbopumps the albedo is 0.993.

In this work, the above described reference simulation was set up without impurity seeding and a deuterium fueling rate of 2.0×10^{22} atoms/s. The deuterium fueling is mimicked by a gas puff of deuterium molecules at the center of the divertor dome baffle, where the divertor valves in ASDEX Upgrade are located. From the reference simulation two sets of simulations were derived. Each features an impurity gas puff from the same divertor location as for deuterium with seeding levels of $\Gamma_N = 1.0 \times 10^{18}$–$1.5 \times 10^{20}$ s^{-1} and $\Gamma_{Ne} = 1.0 \times 10^{18}$–$1.5 \times 10^{19}$ s^{-1} respectively. The impurity seeding rate or the impurity divertor concentration is used as the reference parameter within one set of simulations. In the comparison of simulations with different impurities the integrated power flux to the outer divertor is used as the relevant parameter.

3 Modeling Results

In the simulations, both seeding species produce significant amounts of radiation with radiation fractions similar to those observed in experiments with nitrogen seeding (f_{rad} = 50–80 %) [2]. The power dissipation by line radiation can provide similar power flux density and temperature profiles at the outer target for both seeding species, as seen in Fig. 2. Fig. 3 shows a reduction of the integral power to the outer target along with an increase of the radiated power for increasing scrape-off layer impurity content in the simulations. Despite the rather similar evolution in the integral quantities (Fig. 3.a+b) and similar temperature profiles at the outer target (Fig. 2), the characteristic evolution of the radiation distribution as well as the impact on the upstream plasma parameters differ (Fig. 3.b+c). For nitrogen the upstream separatrix pressure is reduced by 10% in our seeding scan. In contrast, neon decreases the separatrix electron pressure by about 25% when the power to the outer divertor drops below 1 MW ($f_{tar} = 0.125$). With neon seeding the radiation that stems from the main chamber parts of the grid increases from 30 to 50% of the simulated total radiation. For nitrogen this value stays at 30% throughout the scan. Compared to nitrogen, the main chamber radiation profile is shifted radially inwards into the pedestal and core region, whereas nitrogen

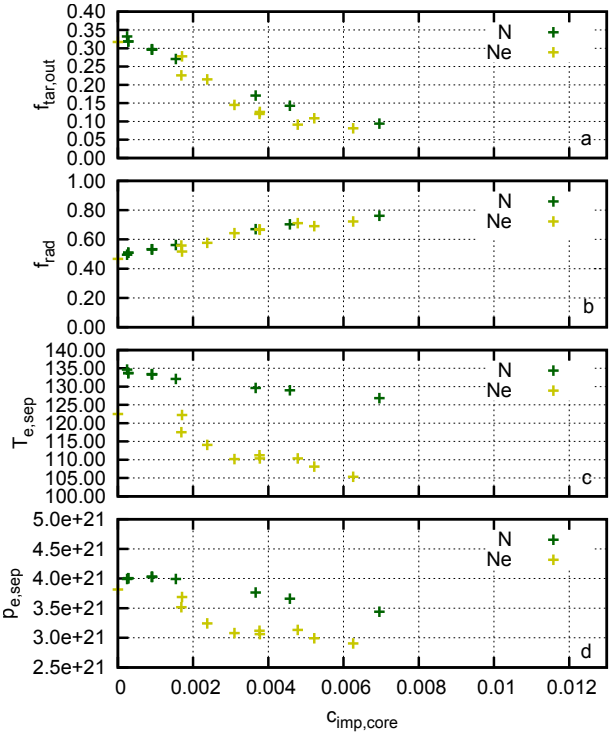

FIG. 3 – The fraction of the power to the outer target (a), the radiated power fraction (b), the outer midplane separatrix electron pressure (c) and temperature (d) are shown for an impurity seeding scan.

radiates dominantly further out in the scrape-off layer. The core radiation fractions in the simulation domain are up to a factor of three higher for neon. In addition, with neon seeding the fraction of radiation from neutrals is significantly larger than for nitrogen seeding. In the divertor there is a clear spatial separation of regions where neon ($T_e > 5$ eV) and deuterium ($T_e \leq 5$ eV) strongly radiate, see Fig. 4. With nitrogen the impurity radiation still contributes to the local power losses also at low electron temperatures. This implies that deuterium power losses via radiation, charge-exchange or recombination are more important for neon seeding to reduce the target temperature to values below 5 eV with the current modeling setup.

The differences for both seeding species are due to at least two reasons. First, the radiation potential L_Z favors main chamber radiation for neon and divertor radiation for nitrogen [14]. Second, divertor enrichment $\eta = \frac{c_{imp,div}}{c_{imp,main}}$ is strong for nitrogen with $\eta =$ 2.5–4.0, whereas for neon divertor enrichment is absent ($\eta = 0.8$–1.2) in the simulations. A similar difference is observed in experimental estimates of divertor enrichment in ASDEX Upgrade experiments [15]. In the modeling, the difference of the enrichment with neon and nitrogen is at least partly due to a change in the relative importance of the thermal and friction forces on the impurity ions. For both impurities the net parallel force on the impurity ions below the X-point points towards the divertor targets. For neon this net parallel force is reduced compared to nitrogen. This leads to a reduction in the parallel density gradient that can be maintained inside the divertor. In addition, the mean free path for neutral impurities is longer for neon neutrals. This leads to a larger fraction of the impurity neutrals recycling at the divertor targets being ionized in the core plasma and in the main chamber scrape-off layer instead of the divertor. The former directly contribute to the impurity content of the confined plasma and the latter leads to a lower content of the impurities in the divertor. For the two simulations shown in Fig. 2 the fraction of the total ionization source is increased from 25% to 48% in the main chamber scrape-off layer and from 0.8% to 8% in the core when comparing nitrogen to neon. The longer mean free path for neon neutrals also implies that the main chamber scrape-off layer is more transparent for the impurity recycling fluxes at the main chamber plasma facing components. In the simulations this leads to a higher ratio, by a factor of about two, of the average concentration in the main chamber scrape-off layer to the average concentration in the confined plasma for nitrogen.

4 Discussion

The presented modeling of a comparative seeding scan with nitrogen and neon as radiative species suggest that the atomic data of nitrogen provides beneficial effects that lead to higher divertor enrichment of the impurity as well as to lower radiation fractions from the confined plasma and lower upstream pressure losses. The stronger impact on the upstream profiles, especially the reduction of the separatrix and pedestal top temperature with neon will reduce the plasma performance. However, the simulations do not reproduce the distinct differences in the initial pedestal response at low seeding rates of nitrogen and neon, which are observed in ASDEX Upgrade experiment. In experiment

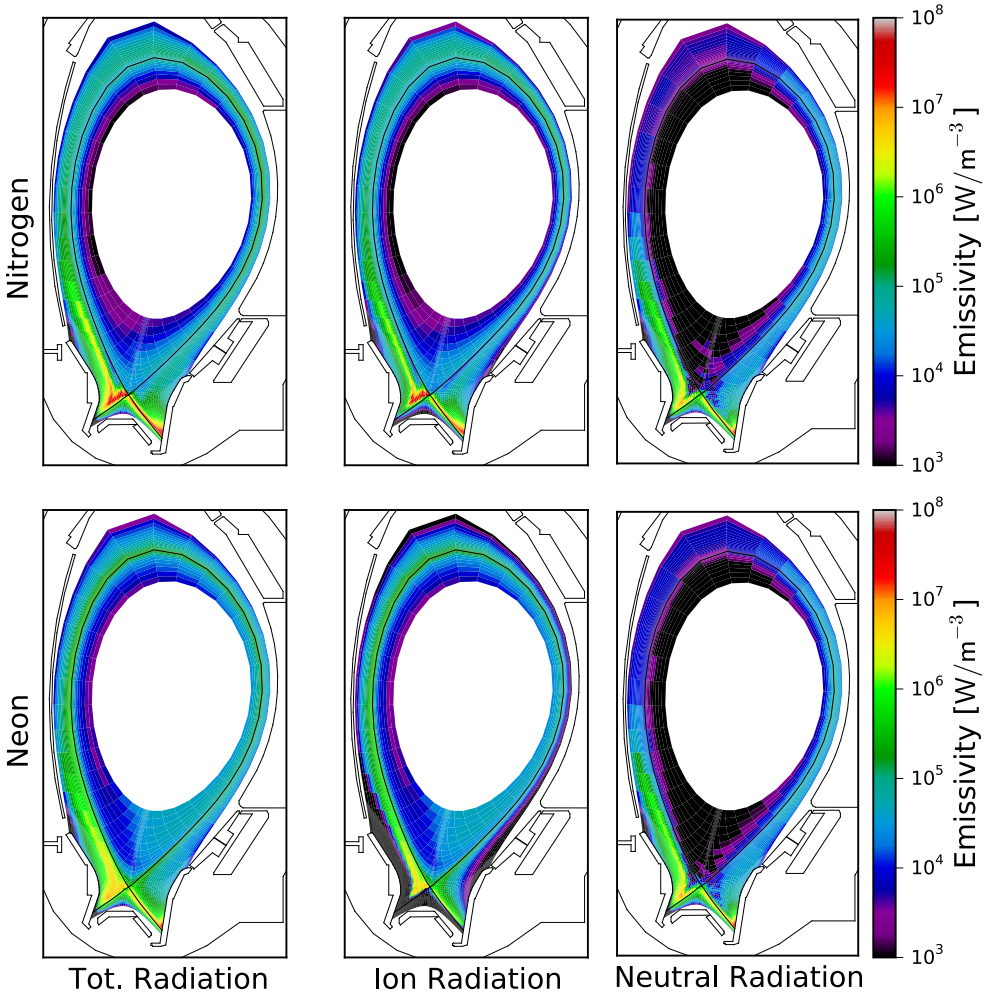

FIG. 4 – The radiation distribution for the nitrogen and neon simulations from Fig. 2 are shown.

nitrogen seeding leads initially to an increase of the pedestal temperature [16] and neon seeding leads initially to an increase in the pedestal density [4]. Such changes seem to be driven by transport effects [17] that are not captured within the presented model. SOLPS simulations of the ITER plasma shows that neon and nitrogen seeding seem to behave very similar in terms of power exhaust. A size scaling of the ASDEX Upgrade simulations is in progress. In future studies it remains to be evaluated if with increasing machine size, hence changing ratio of the mean free path for neutrals to the divertor dimensions, a better enrichment of neon can be achieved.

A particular caveat of the presented analysis is that a different level of sophistication in the atomic data has been used for the volumetric recombination of the impurity species to neutrals. For nitrogen, ADAS data has been employed, whereas for neon the dataset from STRAHL has been used. The latter does not include threebody-recombination and uses a fixed energy loss per recombination event. In effect, the neon simulations will tend to underestimate the amount of recombination into neon neutrals - in particular in the region of high density in the inner divertor. In the simulations a volume of net recombination in front of the inner target exists for nitrogen with sink rates that are comparable to the

local source rates due to ionization further upstream. For neon the local recombination sink rates are suppressed by two orders of magnitude compared to the local ionization source rates. In the cases shown in Fig. 2, the total volumetric recombination sink into nitrogen neutrals is about a fourth of the fluxes to the grid boundaries and is hence a relevant part of the neutral particle source in the simulation. In contrast, for neon this ratio is on the order of 1 %. Future modeling will need to evaluate the impact of a better volume recombination model for neon. It can be expected that the different locations of the production of neutrals as well as the change in their dominant direction of flight can alter the pumping capabilities and the neutral compression of neon.

5 Conclusions

The presented simulations indicate that the use of neon seeding in ASDEX Upgrade for power exhaust is unfavorable as for similar divertor conditions the plasma performance in terms of the separatrix and pedestal top pressure is reduced with respect to simulations with nitrogen seeding. In ASDEX Upgrade experiments neon also features the additional operational challenge of tungsten accumulation that is triggered before the divertor cooling becomes efficient. At this stage a clear extrapolation to ITER is unfortunately not possible without a detailed analysis of the different phenomenology with neon seeding in machines of different size such as ASDEX Upgrade and JET.

Acknowledgments

This work has been carried out within the framework of the EUROfusion Consortium and has received funding from the Euratom research and training program 2014-2018 under grant agreement number 633053. The views and opinions expressed herein do not necessarily reflect those of the European Commission.

References

[1] U. Stroth, et al. *Nucl. Fusion*, 53(10):104003, October 2013.

[2] F. Reimold, et al. *Nucl. Fusion*, 55(3):033004, March 2015.

[3] F. Reimold, et al. *Nuclear Materials and Energy*, submitted, 2016.

[4] M. Bernert, et al. *Nuclear Materials and Energy*, submitted, 2016.

[5] V. Rohde and M. Oberkofler. *Journal of Nuclear Materials*, 463:672–675, August 2015.

[6] D. Neuwirth, et al. *Plasma Phys. Control. Fusion*, 54(8):085008, August 2012.

[7] M. Oberkofler, et al. *Journal of Nuclear Materials*, 438, Supplement:S258–S261, July 2013.

[8] H. D. Pacher, et al. *Journal of Nuclear Materials*, 390–391:259–262, June 2009.

[9] A. S. Kukushkin, et al. *Nucl. Fusion*, 42(2):187, February 2002.

[10] F. Reimold, et al. *Journal of Nuclear Materials*, 463:128–134, August 2015.

[11] V. Kotov, et al. *Plasma Phys. Control. Fusion*, 50(10):105012, October 2008.

[12] A. Scarabosio, et al. *Journal of Nuclear Materials*, 390–391:494–497, June 2009.

[13] M. Wischmeier, et al. *Contrib. Plasma Phys.*, 48(1-3):249–254, March 2008.

[14] A. Kallenbach, et al. *Plasma Phys. Control. Fusion*, 58(4):045013, 2016.

[15] A. Kallenbach. *Nucl. Fusion*, 2016. this conference.

[16] J. Schweinzer, et al. *Nuclear Fusion*, 51(11):113003, November 2011.

[17] M. G. Dunne, et al. In *EPS2015*. European Physical Society, 2015.